Topographic reorganization of cerebrovascular mural cells under seizure conditions

Margarita Arango-Lievano, Badreddine Boussadia, Lucile Du Trieu de Terdonck, Camille Gault, Pierre Fontanaud, Chrystel Lafont, Patrice Mollard, Nicola Marchi, Freddy Jeanneteau

Article

Cell Reports

Topographic Reorganization of Cerebrovascular Mural Cells under Seizure Conditions

Graphical Abstract

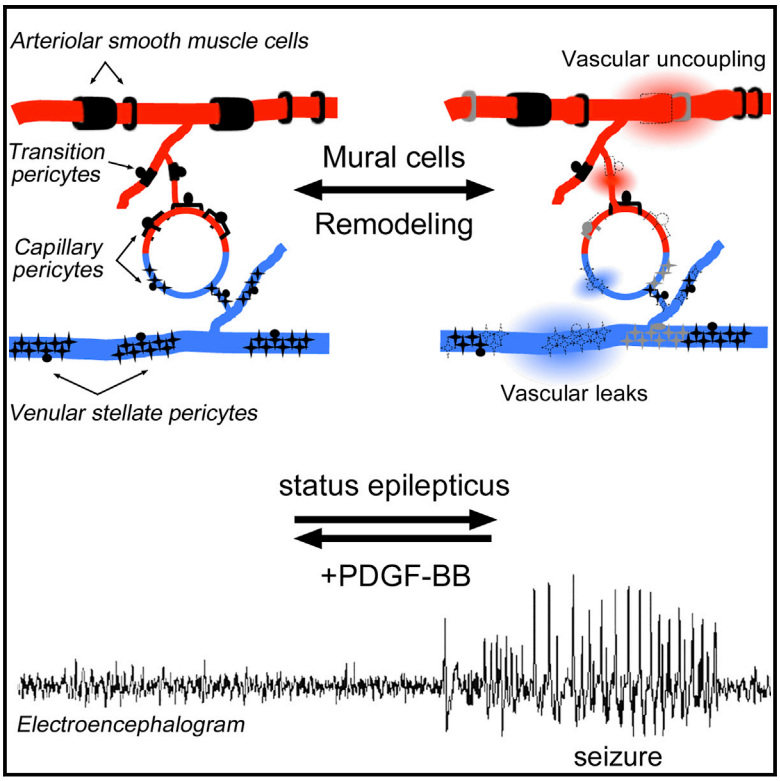

Authors

Margarita Arango-Lievano, Badreddine Boussadia, Lucile Du Trieu De Terdonck, ..., Patrice Mollard, Nicola Marchi, Freddy Jeanneteau

Correspondence

margarita.arango@igf.cnrs.fr (M.A.-L.), nicola.marchi@igf.cnrs.fr (N.M.), freddy.jeanneteau@igf.cnrs.fr (F.J.)

In Brief

Arango-Lievano et al. follow how status epilepticus changes the dynamics of mural cell turnover at the cortical vasculature, causing vessel damage. PDGF-BB, a growth factor promoting the assembly of mural cells at the vascular unit, ameliorates vessel function and reduces spontaneous epileptiform activity.

Highlights

- Turnover of cortical perivascular mural cells is accelerated post-status epilepticus
- Distinct dynamic rates of mural cell addition or elimination cause net deficits
- Mural cell remodeling correlates with vessel pathology
- PDGF-BB reduces mural cell deficits, vessel pathology, and epileptiform activity

Arango-Lievano et al., 2018, Cell Reports *23*, 1045–1059
April 24, 2018
https://doi.org/10.1016/j.celrep.2018.03.110

CellPress

Cell Reports
Article

Topographic Reorganization of Cerebrovascular Mural Cells under Seizure Conditions

Margarita Arango-Lievano,[1,*] Badreddine Boussadia,[2] Lucile Du Trieu De Terdonck,[1] Camille Gault,[1] Pierre Fontanaud,[3] Chrystel Lafont,[3] Patrice Mollard,[3] Nicola Marchi,[2,*] and Freddy Jeanneteau[1,4,*]

[1]Departments of Neuroscience & Physiology, Laboratory of Stress Hormones & Plasticity, Institut de Génomique Fonctionnelle, INSERM, CNRS, University of Montpellier, 34093 Montpellier, France

[2]Department of Neuroscience, Laboratory of Cerebrovascular Mechanisms of Brain Disorders, Institut de Génomique Fonctionnelle, INSERM, CNRS, University of Montpellier, 34093 Montpellier, France

[3]Department of Physiology, Laboratory of Networks and Rhythms in Endocrine Glands, Institut de Génomique Fonctionnelle, INSERM, CNRS, University of Montpellier, 34093 Montpellier, France

[4]Lead Contact

*Correspondence: margarita.arango@igf.cnrs.fr (M.A.-L.), nicola.marchi@igf.cnrs.fr (N.M.), freddy.jeanneteau@igf.cnrs.fr (F.J.)

https://doi.org/10.1016/j.celrep.2018.03.110

SUMMARY

Reorganization of the neurovascular unit has been suggested in the epileptic brain, although the dynamics and functional significance remain unclear. Here, we tracked the *in vivo* dynamics of perivascular mural cells as a function of electroencephalogram (EEG) activity following status epilepticus. We segmented the cortical vascular bed to provide a size- and type-specific analysis of mural cell plasticity topologically. We find that mural cells are added and removed from veins, arterioles, and capillaries after seizure induction. Loss of mural cells is proportional to seizure severity and vascular pathology (e.g., rigidity, perfusion, and permeability). Treatment with platelet-derived growth factor subunits BB (PDGF-BB) reduced mural cell loss, vascular pathology, and epileptiform EEG activity. We propose that perivascular mural cells play a pivotal role in seizures and are potential targets for reducing pathophysiology.

INTRODUCTION

Cerebrovascular dysfunction is a hallmark of diseases of the CNS, either as a pathophysiological cause or as a consequence (Friedman, 2011). Disruption of barrier functions at the cerebrovasculature provokes a disarray of exchanges between brain parenchyma and blood that can alter the homeostasis of neuronal networks associated with seizures (van Vliet et al., 2007; Fabene et al., 2008), along with hippocampal or cortical atrophy, neuronal loss, and behavioral changes (Bell et al., 2010; Hall et al., 2014; Winkler et al., 2012). Studies of cerebrovascular permeability in seizure disorders have focused on endothelial cells as cellular culprits, neglecting the multi-cellular nature of the cerebrovasculature and overlooking intercellular defects occurring at the perivascular compartment (Gorter et al., 2015; Attwell et al., 2010). The perivascular mural cells, pericytes, and vascular smooth muscle cells (VSMCs) establish a functional network with astrocytes and endothelial cells, contributing to neurovascular coupling (Sweeney et al., 2016; Hall et al., 2014; Hill et al., 2015; Whiteus et al., 2014). Pericyte deficiency is implicated in several CNS disorders featuring barrier disruption (Winkler et al., 2011), yet it is mainly overlooked in seizure disorders. Pericytes, VSMCs, and endothelial cells form a physical and chemical barrier that controls the passage of fluids, ions, and molecules between milieu, thereby maintaining the proper environment for neural cells and protecting them from toxins and pathogens (Daneman and Prat, 2015).

We and others have shown changes in pericyte morphology in human cortex and hippocampus of drug-resistant epileptic patients affected by temporal lobe epilepsy and focal cortical dysplasia (Garbelli et al., 2015; Liwnicz et al., 1990). However, the impact of seizures on the turnover of pericytes has not been explored. It is unknown whether mural cell remodeling associates with vascular lesions known to be epileptogenic (Awad and Jabbour, 2006; Cocito et al., 1982). Arteriovenous lesions encountered in epilepsy surgery patients can be associated with calcification, rigidity, and permeability (Pinto et al., 2016). The latter is relevant for the pericytes, because they contribute to vessel calcification, tonus defects, and permeability, all previously linked to loss-of-function mutations in the platelet-derived growth factor subunits BB (PDGF-BB) pathway (Keller et al., 2013; Lindahl et al., 1997; Ouyang et al., 2018).

PDGF-BB signaling via platelet-derived growth factor receptor (PDGFR) β at the interface between the pericytes and the endothelium has been implicated in angiogenesis, vessel stabilization, blood flow regulation, barrier functions, tissue repair, and regeneration (Winkler et al., 2011; Sweeney et al., 2016). Knockout studies in mice showed that PDGF-BB signaling is essential for the maintenance of cerebrovascular integrity and for survival (Armulik et al., 2010; Daneman et al., 2010). Partial deficit of PDGF-BB in heterozygous mice is sufficient to affect blood-brain barrier (BBB) permeability (Armulik et al., 2010; Daneman et al., 2010), cerebral microcirculation, parenchyma oxygenation, and neuronal survival (Winkler et al., 2010; Kisler et al., 2017; Hall et al., 2014). Transient antagonism of PDGFRβ signaling in the retina is also sufficient to breakdown the retina-blood barrier, associated with pericyte deficiency, microbleeds, hypoperfusion, and inflammation (Ogura et al., 2017; Park et al., 2017). In general, these results posit PDGF-BB as a candidate trophic factor for the mural cells to promote barrier functions.

We present a longitudinal study of mural cell dynamics in mouse cortex using *in vivo* two-photon microscopy, coupled with time-lapse analyses of blood flow and vessel tonus and electroencephalogram (EEG) recordings to track cerebrovascular remodeling, following status epilepticus and after treatment with PDGF-BB.

RESULTS

Status Epilepticus-Induced Vascular Damage in the *In Vivo* Imaging Region of Interest

To investigate the dynamics of mural cells under seizure conditions, we first examined whether the cortex that we intend to image presents vascular damage post-status epilepticus. To visualize microbleeds into the brain parenchyma, we injected mice with fluorescent tracers, intravenously, before induction of convulsive status epilepticus with systemic kainate injection (Figure S1A). Parenchymal leaks of Evans blue (EB) or 10-kDa dextran-Alexa 568 were found in all layers of the cortex (Figures S1B and S1C). Leakage sites associated with reactive glia and parenchymal cells were loaded with dextran dye (Figures S1D–S1F).

Dynamic Remodeling of Vascular Mural Cells Post-Status Epilepticus

The mural cell vascular unit (Figure 1A) is visualized over several hundred square microns (Figure 1B) at various time points post-status epilepticus with a transcranial technique in transgenic *NG2-tomato* mice injected into the circulation with 70-kDa dextran-fluorescein isothiocyanate (dextran-FITC). Keeping the skull is important for accurate measures of vascular dynamic signals, because craniotomy causes inflammation (Lagraoui et al., 2012), neovascularization (Drew et al., 2010), heartbeat pulsation-related movement artifacts (Paukert and Bergles, 2012), improper hemodynamics (Drew et al., 2010), neuroplasticity defects (Xu et al., 2007), and cortical spreading depression (Chang et al., 2010). Thus, we captured the topology of mural cell changes on the cortical vasculature through a thin-skull preparation (Figure 1C). We found that convulsive status epilepticus induced long-term remodeling of NG2 mural cells at large pial and penetrating vessels, as well as capillaries (Figure 1D). In contrast, mice that did not develop convulsive status epilepticus presented reversible remodeling of NG2 mural cells on the large and small vessels (Figure S2). The overall mural cell coverage decreased merely early post-status epilepticus (Figure 1E) compared to control mice (Figure 1F), indicating that mural cell topology remodeling may vary as a function of status epilepticus severity.

Remodeling of Mural Cells Is Proportionate to Status Epilepticus Severity

Subtypes of mural cells are distinguished in *NG2-tomato* mice based on their morphology (Hill et al., 2015), uptake of neuroTrace (Damisah et al., 2017), expression of alpha-smooth muscle actin (α-SMA), and location on endomucin-coated vessels: the ring-like VSMCs express α-SMA on endomucin-uncoated arterioles, the transition pericytes on endomucin-uncoated pre-capillary arterioles, the ensheathing pericytes on endomucin-coated capillaries, and the stellate pericytes on post-capillary endomucin-coated venules (Figure 2A).

To determine the dynamic rates of remodeling for each mural cell subtype as a function of status epilepticus severity, we imaged mural cells (Figures 2B–2E) and recorded EEG activity in the same mice over time (Figures 2F and 2G). Gains and losses of pericytes and VSMCs on the vasculature (Figure 2B) were consistent with co-labeling of *NG2-tomato* mural cells with markers of proliferation (antigen recognized by monoclonal antibody KI-67 [KI67], 7/2,067 cells on day 14 and 9/2,004 cells on day 44) and death (cleaved caspase-3 [CC3], 11/2,007 cells on day 14 and 4/2,011 cells on day 44) (Figure 2C). Most changes persisted over time and gradually unfolded post-status epilepticus (Figure 2D). For pericytes, gains offset the losses, causing minimal net changes (Figure S3). For VSMCs, gains and losses were out of phase, causing net changes of vascular coverage (Figure S3). The extent of remodeling differed according to the NG2 cell subtype: a small proportion of arterioles exhibited remodeling of VSMCs in large clusters, whereas a large proportion of capillaries featured small changes of pericytes (Figure 2E). Overall, the remodeling of mural cells correlated with the severity of status epilepticus at induction (Figure 2G). For comparison, control mice showed minimal dynamics of mural cells (Figure 2D; Figure S3) and none of the *NG2-tomato* cells co-stained with KI67 or cleaved caspase-3.

Significance of Mural Cell Turnover

To assess the impact of mural cell remodeling post-status epilepticus, we measured changes of vessel diameter between time points. Arterioles and capillaries responded almost uniformly to mural cell additions by a reduction of vessel diameter and to mural cell eliminations by an augmentation of vessel diameter (Figures 3A and 3B). In contrast, venules did not change diameter after gains and losses of stellate pericytes (Figure 3C).

Vessel anomalies coincided with gains and losses of mural cells post-status epilepticus, persisting throughout the imaging sessions (Figure 3D). Reversible aneurysms associated with regrowth of NG2 mural cell coverage (Figure 3A, examples 3, 5, and 6), whereas the persistent aneurysms associated with persistent losses of VSMCs (Figure 3A, examples 1 and 2). Topologically, vessel anomalies occurred on pre-capillary arterioles and on capillaries (Figure 3E). Altogether, these results indicate that vessel anomalies are linked to the remodeling of NG2 mural cells, and strategies to maintain these cells post-status epilepticus could be beneficial.

PDGF-BB Stimulates Mural Cell Growth Post-Status Epilepticus

To favor the growth and maintenance of mural cell coverage, we examined the effect of PDGF-BB *in vivo*. Intravenous administration of PDGF-BB promoted the phosphorylation of PDGFRβ in cortex (Figure 4A). Treatment delivery commenced post-status epilepticus and lasted 2 weeks (Figure 4B) on mice developing convulsive status epilepticus (2 groups: saline and PDGF-BB) compared with naive controls. Treatment with PDGF-BB promoted growth of mural cells post-status epilepticus (Figures 4C–4E) and reduced the number of aneurysm-like changes (Figure 4F) that were not associated with the mere net gains of stellate pericytes (Figure S4), at least topologically (Figure 4G).

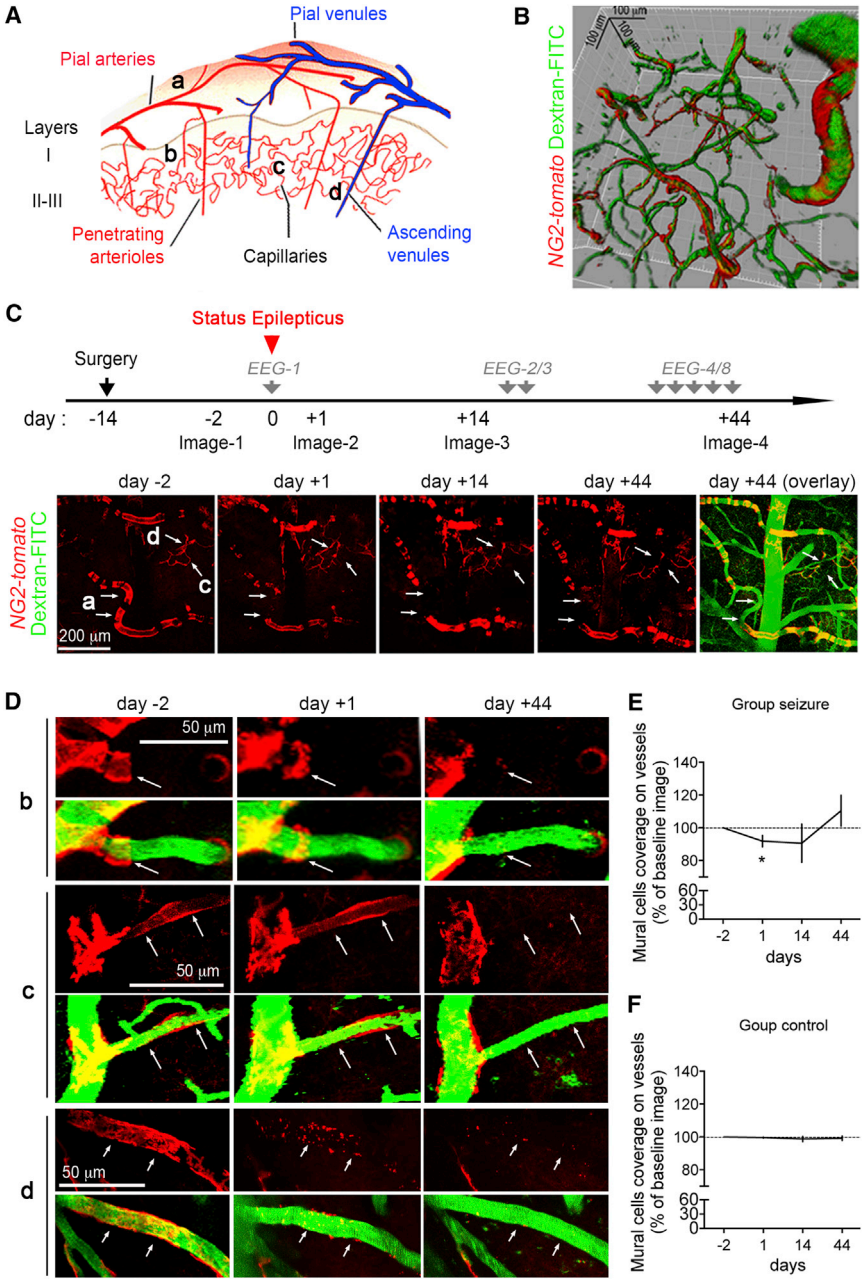

Figure 1. Seizure-Induced Remodeling of Vascular Mural Cells in Living Mouse Cortex

(A) Schematic representation of vessel topology in parietal cortex, which drains blood from large penetrating arterioles through small-diameter capillaries to large ascending veins on the pial surface. Inset letters show vessel subtype categories displayed in two-photon images. See Figure S1.

(B) 3D reconstruction of a cortical volume imaged through a thinned skull window in *NG2-tomato* transgenic mice under anesthesia. Vascular mural cells are labeled with *tomato*, and vessels are labeled with intravenous 70-kDa dextran-FITC.

(C) Experimental timeline. Surgical implantation of cortical electrodes was followed by 2 weeks of recovery with subsequent sessions of EEG recordings in freely moving mice and transcranial imaging of parietal cortex before and after induction of seizures with kainic acid (injected intraperitoneally at 25 mg/kg) on day 0. Representative cortical volume imaged in the same mouse before and after induction of seizures reaching convulsive status epilepticus. Arrows indicate mural cell remodeling at distinct vessel categories (refer to inset letters).

(D) Persistent remodeling of NG2 mural cells post-status epilepticus. Examples of arteriole (b), post-capillary venule (c), and venule (d). This contrasts with the reversible remodeling of NG2 mural cells in mice experiencing seizures but no status epilepticus. See Figure S2.

(E) Percentage of mural cell coverage on vessels after status epilepticus. Means ± SEM of n = 25 mice at day −2 and day +1, n = 11 mice at day +14, and n = 12 mice at day +44 (unpaired t test comparing day +1 and baseline at day −2, *p < 0.02).

(F) Percentage of mural cell coverage on vessels in controls. Means ± SEM of n = 8 mice at all time points.

Functional Dynamics of Mural Cells

One question remains: whether the cerebrovasculature is healthier after treatment with PDGF-BB compared to saline. To address this question, we imaged non-invasively blood flow at sites of mural cell remodeling. To this end, we used the thin-skull preparation to spot mural cell remodeling (Figure 5A), which we imaged with intravenous 70-kDa dextran-Texas red to track blood cell velocity (Figure 5B). Vessel categories are easily recognized by the direction of flow: (1) from big to small vessels in arteries and (2) from small to big vessels in veins. Group data from multiple vessels in anesthetized control mice showed that basal blood flow is proportionate to vessel caliber regardless of vessel coverage with NG2 mural cells (Figure 5C). Post-status epilepticus, small-caliber vessels with NG2 cell coverage increased blood flow velocity (Figure 5C), an effect corrected by treatment with PDGF-BB (Figures 5C and 5D).

To further determine the effect of PDGF-BB treatment on vasoregulation, we used a known vasodilator (glutamate) (Hall et al., 2014) and vasoconstrictor (ET-1) (Dehouck et al., 1997), because its endothelin receptor type A (EDNRA) is enriched in mural cells (He et al., 2016). We used the cohort of mice described in Figure 5A for time-lapse two-photon microscopy of vessel tonus in response to glutamate (GLU) and ET-1 applied topically through a cranial window, precisely at sites of mural cell remodeling post-status epilepticus (Figure 5E). We found glutamate-evoked dilation of capillaries accompanied by glutamate-evoked contraction on pre-capillary arterioles of control mice (Figure 5F), an effect more robust at vessels covered with NG2 cells than at uncovered vessels

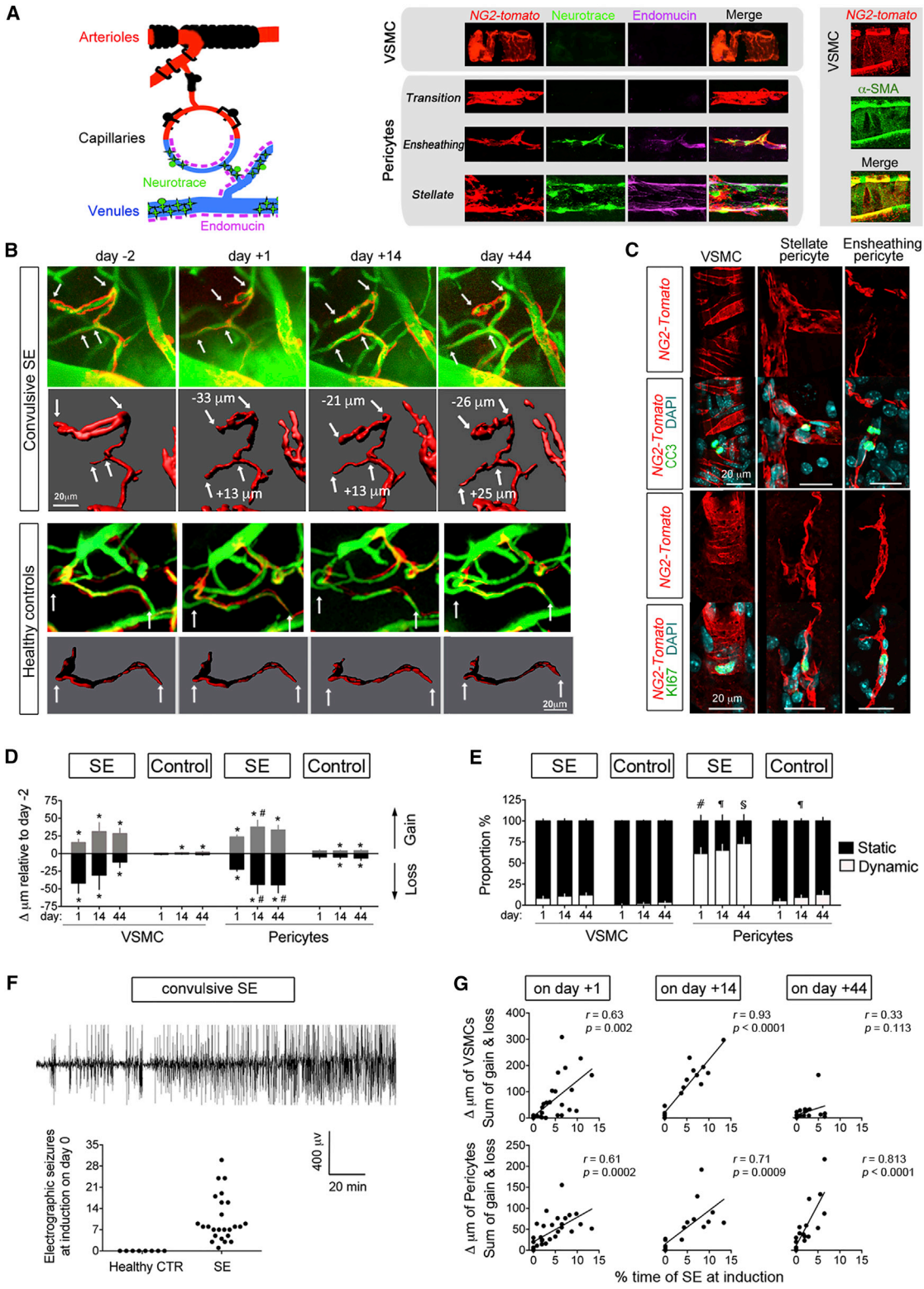

Figure 2. Remodeling of NG2 Mural Cells Is Proportionate to the Severity of Status Epilepticus at Induction

(A) Characterization of mural cell subtypes at the cortical vasculature of *NG2-tomato* mice. VSMCs and pericytes subtypes (transition, capillary, and stellate) are sorted by morphology, uptake of neuroTrace, expression of α-SMA, and localization on endomucin$^+$ vessels.

(legend continued on next page)

(Figure 5G). ET-1 uniformly caused contraction of all vessels, except capillaries and post-capillary venules (Figure 5F), with a longer-lasting effect if vessels were covered with NG2 cells rather than uncovered (t test, t = 23 min versus t = 37 min for NG2 covered, p = 0.0016, and for NG2 uncovered, p = 0.65) (Figure 5G). There was no difference in tonus regardless of whether vessels were always covered with NG2 cells or gained coverage post-status epilepticus (Figure 5F). Likewise, there was no difference in tonus regardless of whether vessels were never covered with NG2 cells or lost coverage post-status epilepticus (Figure 5F).

Vessel tonus to glutamate and ET-1 was reduced and delayed post-status epilepticus, an effect that was partially corrected by treatment with PDGF-BB (Figure 5G; Figures S4C and S4D). Altogether, we conclude that treatment with PDGF-BB restored vasomodulatory functions.

Venular Tropism of PDGF-BB Effects Post-Status Epilepticus

One question that remains unanswered is why the post-capillary venules overgrow stellate pericytes upon PDGF-BB treatment. First, we looked at whether the response of PDGF-BB receptor changes as a function of vessel subtypes and caliber. Phosphorylation of PDGFRβ is prominent on penetrating arterioles and capillaries (harboring α-SMA$^+$ cells) and to a lesser extent on ascending veins and post-capillary venules (endomucin$^+$ segments) in control mice and post-status epilepticus (Figure 6A). In contrast, treatment with PDGF-BB post-status epilepticus increased the proportion of venules harboring phosphorylated PDGFRβ (p-PDGFRβ) compared to the saline group (Figure 6B). This could result from the upregulation of PDGFRβ expression post-status epilepticus. Instead, we found a downregulation in the mural cells at venules compared to arterioles after PDGF-BB treatment (Figure 6C; Figures S5A–S5C), indicating that phosphorylation of PDGFRβ did not correspond with excess PDGFRβ expression.

This prompted us to examine the impact of PDGF-BB on cerebrovascular permeability. Using the fluorescent tracer approach (Figure S1), we found fewer extravasation spots on capillaries and post-capillary venules (endomucin$^+$/α-SMA$^-$ vessels) of mice treated with PDGF-BB compared to saline controls (Figure 6D), indicative of a topographic reorganization of leaks at the cortical vasculature (Figure 6E). Overall, PDGF-BB treatment associated with a reduction of microbleeds in terms of the surface of leakage spots (Figure 6F), the number of parenchymal cells with dye (Figure 6G), and reactive microglia (Figures S5C and S5D). These data indicate that PDGF-BB treatment post-status epilepticus reduced cortical vascular damage with a tropism for capillaries and post-capillary venules.

Effect of PDGF-BB Treatment on EEG Activity

Finally, we explored the impact of PDGF-BB on EEG activity (Figures 7A–7C). There was a marked reduction of spontaneous EEG epileptiform activity in the PDGF-BB group compared to the saline group at 2 weeks post-status epilepticus despite similar EEG activity between groups at induction. To assess whether treatment modified the relationship between mural cell remodeling and EEG activity, we correlated the net change of mural cells with seizures (Figure 7D), spikes (Figure 7E), and epileptiform events (Figure 7F). At 2 weeks post-status epilepticus, spontaneous EEG activity correlated with mural cell loss on arterioles and capillaries except in mice treated with PDGF-BB. At 6 weeks post-status epilepticus, spontaneous EEG epileptiform activity declined to almost zero in both groups and no longer correlated with mural cell remodeling (Table S6). This suggests that PDGF-BB modified the course of neuropathology during treatment.

DISCUSSION

Here, we tracked the functional *in vivo* dynamics of mural cells as a function of EEG activity following convulsive status epilepticus as an initial insult. We report that intravenous PDGF-BB activated PDGFRβ in mural cells, ameliorating vessel coverage with mural cells, vessel functions, and reducing spontaneous EEG epileptiform activity.

Topology of Mural Cell Plasticity and Cerebrovascular Dysfunction in Epilepsy

Although the literature dealing with vascular mechanisms of epilepsy focused on capillary BBB, our results point to a pathophysiological role of all cerebrovascular segments. We report several principles of plasticity governing mural cell dynamics in the living cortex under resting and seizure conditions: (1) mural cells are continuously added and removed from the cortical

(B) 3D reconstruction of the pericyte network remodeled in cortex post-status epilepticus compared to healthy controls. Sites of pericyte remodeling (net change of vessel coverage in microns) are accompanied by changes of vessel perfusion with dextran-FITC. Scale bar, 20 μm.
(C) Representative *NG2-tomato* mural cell subtypes post-status epilepticus co-labeled with markers of apoptotic cell death (cleaved caspase-3) or cell proliferation (KI67).
(D) Vessel coverage with *NG2-tomato* mural cells (mural cell length on its vessel/total length of vessel segment) expressed as gains and losses compared to the first imaging session on day −2 (157 vessels harboring VSMCs and 346 vessels harboring pericytes). Means ± SEM of n = 25 status epilepticus mice and 8 control mice (unpaired t test comparing time points post-status epilepticus with day −2, *p < 0.03, and paired t test comparing day +1 with consecutive time points post-status epilepticus, #p < 0.04). See Figure S3.
(E) Proportion of mural cell subtypes rearranged after induction of convulsive status epilepticus at 157 vessels harboring VSMCs and 346 vessels harboring pericytes. Means ± SEM of n = 25 status epilepticus mice and 8 healthy controls (unpaired t test comparing dynamics of VSMCs versus pericytes on day 1, #p < 0.0001, and on day 14, ¶p < 0.0001; post-status epilepticus on day 14, ¶p = 0.0033; and in controls on day 44, §p < 0.0001).
(F) Kainic acid-induced electrographic status epilepticus recorded by EEG, and convulsive as monitored by video tracking. The number of status epilepticus was monitored within 3 hr post-induction in 25 status epilepticus mice and 8 healthy controls.
(G) Pearson correlation between the remodeling of *NG2-tomato* mural cells (sum of gains and losses) and the severity of status epilepticus at induction expressed as duration (percentage of recorded time). Among the 25 status epilepticus mice and 8 controls, all were analyzed longitudinally on day +1, 11 status epilepticus mice and 7 controls were analyzed on day +14, and 12 status epilepticus mice and 7 controls were analyzed on day +44.
See Table S1.

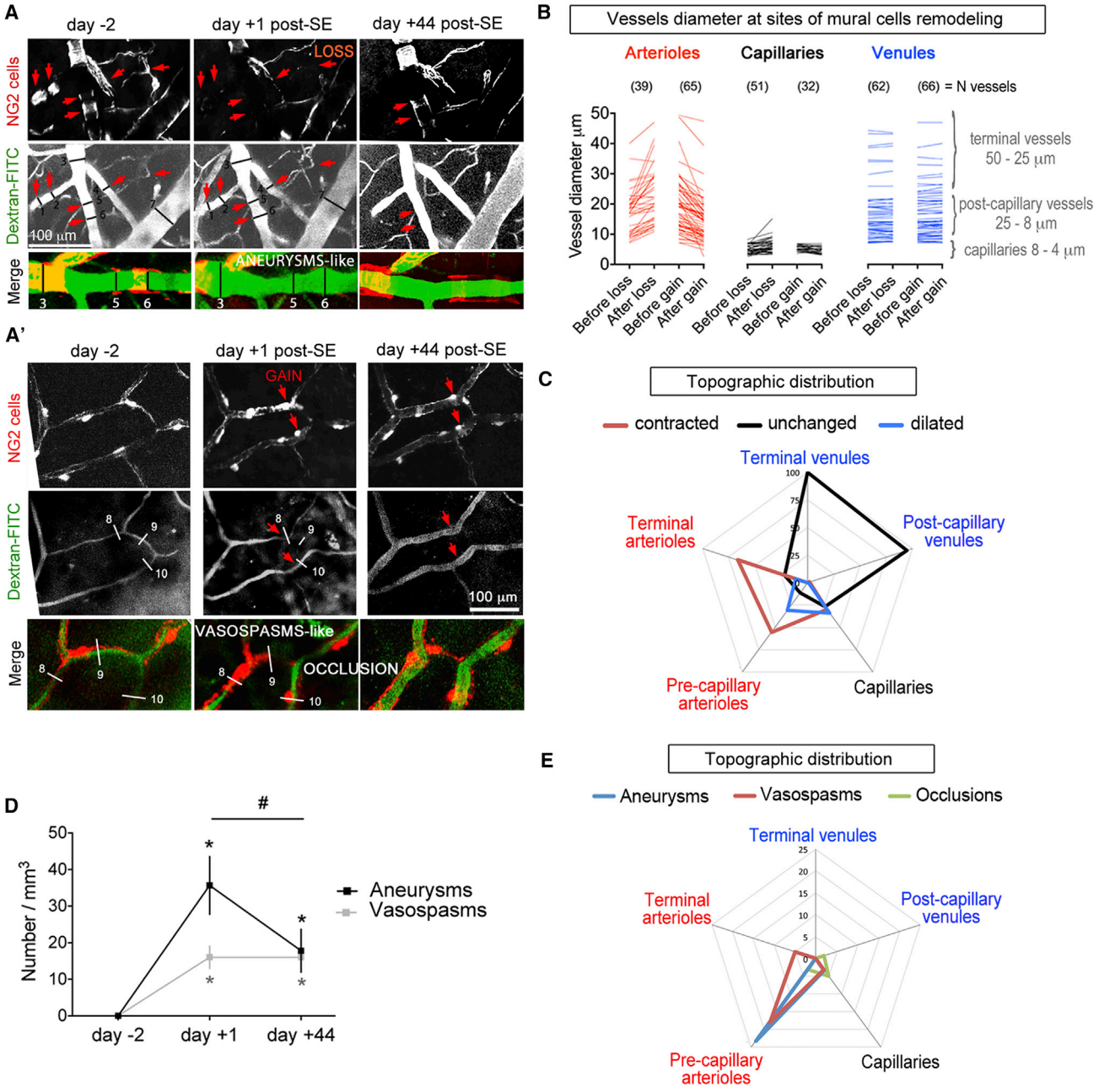

Figure 3. Impact of Mural Cell Remodeling on the Cortical Vasculature

(A) Effect of mural cell loss on vessel diameter at cross-section lines 3, 5, and 6 show aneurysm-like abnormalities where VSMCs disappeared, which reverted with VSMC growth. (A') Effect of mural cell gain on vessel diameter. Lines 8 and 10, vasospasm-like abnormalities; line 9, vessel occlusion.

(B) Vessel diameters at sites of mural cell remodeling at 322 vessels in 19 mice between day −2 and day +1.

(C) Proportion of vessels changing diameter above the 10% cutoff after the gain or loss of *NG2-tomato* mural cells at 101 arterioles, 93 capillaries, and 129 venules sorted as a function of vessel caliber: terminal vessels (25–50 μm), pre- or post-capillaries (8–25 μm), and capillaries (4–8 μm) in 19 mice.

(D) Persistence of abnormalities at 52 vessels after induction of convulsive status epilepticus. Means ± SEM of n = 11 mice (unpaired t test comparing day −2 and day +1, *p < 0.0001; day −2 and day +44, *p = 0.0032; and day +1 and day +44, #p = 0.042).

(E) Vessel abnormalities associated with *NG2-tomato* mural cell remodeling sorted as a function of vessel caliber. n = 322 vessels.

See Table S2.

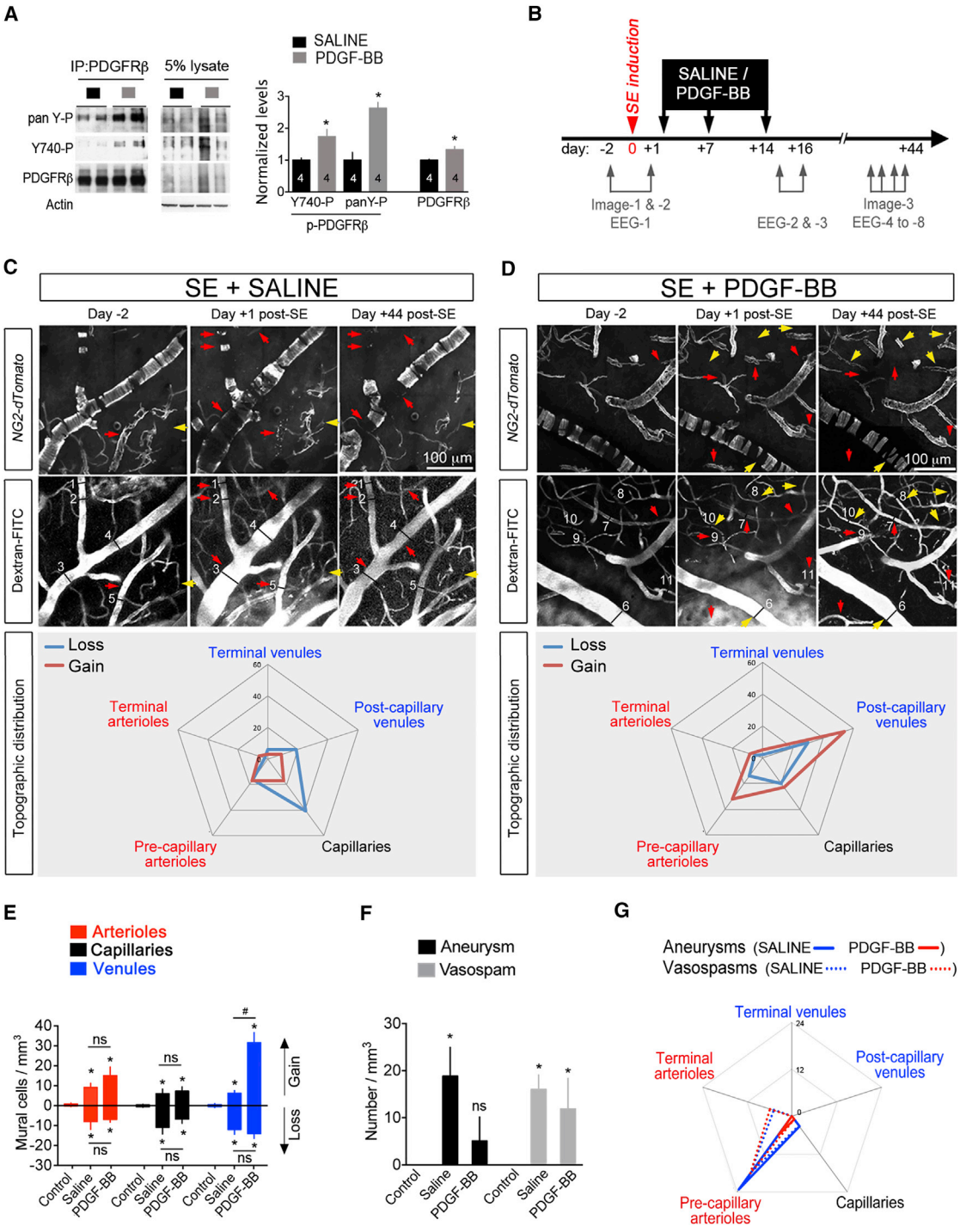

Figure 4. Promoting Growth of NG2 Mural Cells with PDGF-BB

(A) Activation of PDGFRβ (Y740-P and pan-Y-P) on immunoprecipitates of PDGFRβ in mouse cortical lysates collected after a single intravenous injection of 100 μg of PDGF-BB compared to saline-injected controls. Means ± SEM of n = 4 mice (unpaired t test for Y740-P, *p = 0.018; for pan-Y-P, *p = 0.0016; and for PDGFRβ; *p = 0.015).

(B) Timeline of treatment: once a week for 3 consecutive weeks starting after the 2nd imaging session on day +1.

(C) Remodeling of vessel coverage with *NG2-tomato* mural cells post-status epilepticus in mouse cortex before and after treatment with saline. Arrows indicate gains (yellow) and losses (red) of mural cells. Cross-section lines 3 and 4, aneurysm-like; line 6, vasospasm-like abnormalities. Changes of mural cells in 322 vessels of 11 mice are sorted as a function of caliber: terminal vessels (25–50 μm), pre- or post-capillaries (8–25 μm), and capillaries (4–8 μm). See Figure S4A.

(legend continued on next page)

vasculature, (2) venules and arterioles are capable of mural cell plasticity, (3) turnover rates are different among mural cell subtypes, and (4) mural cell addition or removal is associated with changes in resting diameter at arteriolar and capillary vessels.

Pericytes are heterogeneous mural cells sorted as transitional, ensheathing, and stellate subtypes according to morphology and distribution on the vasculature (Kisler et al., 2017). Specific markers are lacking to investigate molecular mechanisms in each subtype. Mural cells in brain have both mesoderm and neuroectoderm origins (Winkler et al., 2011). Our study specifically investigated the NG2 mural cells derived from the mesoderm progenitor cells (Armulik et al., 2011).

Persistent remodeling of mural cell vascular coverage is consistent with the proliferation and death of NG2 cells post-status epilepticus in contrast to the reversible remodeling of mural cells in mice that experienced EEG seizures but no status epilepticus. Death of pericytes was previously associated with neurovascular uncoupling in retina and cortex (Attwell et al., 2010; Hill et al., 2015). We found an acceleration of blood flow in NG2-covered capillaries 2 weeks post-status epilepticus that could result from neurovascular uncoupling. The latter is relevant to seizure activity, in which changes of neurovascular coupling reflect ictal to inter-ictal transitions, associated to differential perfusion and bold magnetic resonance (MR) signals (Hall et al., 2014). But we also report capillary occlusions post-status epilepticus in which pericytes rearranged, as previously described in ischemic vessels with no reflow linked to pericyte death (Hall et al., 2014).

The functional topology of the mural cell network at the cortical vasculature is characterized by (1) the subtype of mural cell involved and (2) the caliber of vessel involved. Remodeling of VSMCs on penetrating arterioles that source the neocortical microvasculature could affect the robustness of the perfusion domain (Blinder et al., 2010). Remodeling of the ensheathing pericytes on the capillary bed that sustains the bulk exchange of metabolites and gases between blood and brain could affect neuronal homeostasis and survival (Whiteus et al., 2014). Remodeling of the stellate pericytes on the ascending veins could affect the clearance of parenchymal wastes and perturb tissue homeostasis.

We report that topical application of glutamate to the cortex evoked a dilation of capillaries and a contraction of arterioles that could optimize blood perfusion regionally. Communication between mural cell subtypes on capillaries and upstream arterioles via Ca^{2+} waves has been previously involved in neurovascular coupling (Peppiatt et al., 2006). Responses of arterioles and capillaries to glutamate and ET-1, whose receptor is mainly expressed in mural cells (He et al., 2016), were hampered post-status epilepticus, rendering vessels stiffer upon treatments with vasoregulating drugs. This could explain the vascular insufficiency associated with seizure disorders (Farrell et al., 2017).

Deciphering Arterial versus Venule Cell Changes Consequent to Status Epilepticus

The differential impact of seizure activity on cortical arterial and venular vessels has been overlooked. On arterioles, net changes of vascular coverage shortly after status epilepticus extended over tens of microns on the pial and penetrating vessels where VSMCs were added or removed in clusters. On capillaries, remodeling of pericytes was frequent but never in clusters, extending over a few microns and resulting in minimal impact on vessel coverage. On venules, the eliminations of pericytes were more frequent at the pial surface and ascending vessels, where hundreds of microns of endothelium lost pericyte coverage post-status epilepticus.

Time-lapse imaging of the same mural cells over time revealed that eliminations of VSMCs preceded growth on the same vessel or neighboring vessel, suggesting that mechanisms of additions and eliminations are temporally dissociated. Additions of new VSMCs could be compensatory for adjusting vasoregulation in the surrounding tissue. Consistently, arteriolar tonus and blood flow are impaired 2 weeks post-status epilepticus when there is net loss of VSMCs. Because they express α-SMA, VSMCs are primary candidates for assuming the role of vasoconstriction on arterioles and change perfusion rate pertaining to the neurovascular coupling (Hill et al., 2015). The roles of the α-SMA^{-} mural cells, distributed on capillaries and veins, remain elusive (Damisah et al., 2017). Stellate pericytes have been attributed vascular barrier functions (Hartmann et al., 2015). The distribution of vascular leakage post-status epilepticus equally associated with endomucin^{+} and α-SMA^{+} vessels argues against a functional tropism. However, endomucin^{+} post-capillary venules are primary sites of leukocyte infiltration across the BBB (Proebstl et al., 2012), and

(D) Remodeling of vessel coverage with *NG2-tomato* mural cells post-status epilepticus before and after treatment with PDGF-BB. Arrows indicate gains (yellow) and losses (red) of mural cells. Cross-section line 11 indicates vascular occlusion. Changes of mural cells in 279 vessels of 8 mice are sorted as a function of caliber: terminal vessels (25–50 μm), pre- or post-capillaries (8–25 μm), and capillaries (4–8 μm). See Figure S4A.

(E) Gains and losses of *NG2-tomato* mural cells in the same cortical volume between day +1 and day +44. Means ± SEM of n = 8 controls, 11 status epilepticus + saline mice, and 8 status epilepticus + PDGF-BB mice. Effects of status epilepticus + saline compared to controls (unpaired t test for gains on arterioles, *p = 0.002; capillaries, *p = 0.0038; and veins, *p = 0.0016, and for losses on arterioles, *p = 0.038; capillaries, *p = 0.0086; and veins, *p = 0.0005). Effects of status epilepticus + PDGF-BB compared to controls (unpaired t test for gains on arterioles, *p = 0.0031; capillaries, *p = 0.0032; and veins, *p < 0.0001, and for losses on arterioles, *p = 0.002; capillaries, *p = 0.046; and veins, *p < 0.0001). Effect of PDGF-BB compared to saline (unpaired t test for gains on veins, #p < 0.0001). Effect of PDGF-BB on the net changes of pericytes on veins post-status epilepticus (unpaired t test, #p < 0.0001). See Figure S4B.

(F) Effect of PDGF-BB treatment on the number of aneurysms and vasospasms post-status epilepticus at 84 vessels (52 status epilepticus + saline mice and 32 status epilepticus + PDGF-BB mice) between day +1 and day +44. Means ± SEM of n = 8 controls, 11 status epilepticus + saline mice, and 8 status epilepticus + PDGF-BB mice (unpaired t test comparing controls with the saline group for aneurysms, *p = 0.026, and vasospasms, *p = 0.0002, and comparing controls with the PDGF-BB group for aneurysms, *p = 0.5, and vasospasms, *p = 0.044).

(G) Vessel abnormalities at 322 vessels of 11 status epilepticus + saline mice and at 279 vessels of 8 status epilepticus + PDGF-BB mice sorted as a function of caliber: terminal vessels (25–50 μm), pre- or post-capillaries (8–25 μm), and capillaries (4–8 μm).

See Table S3.

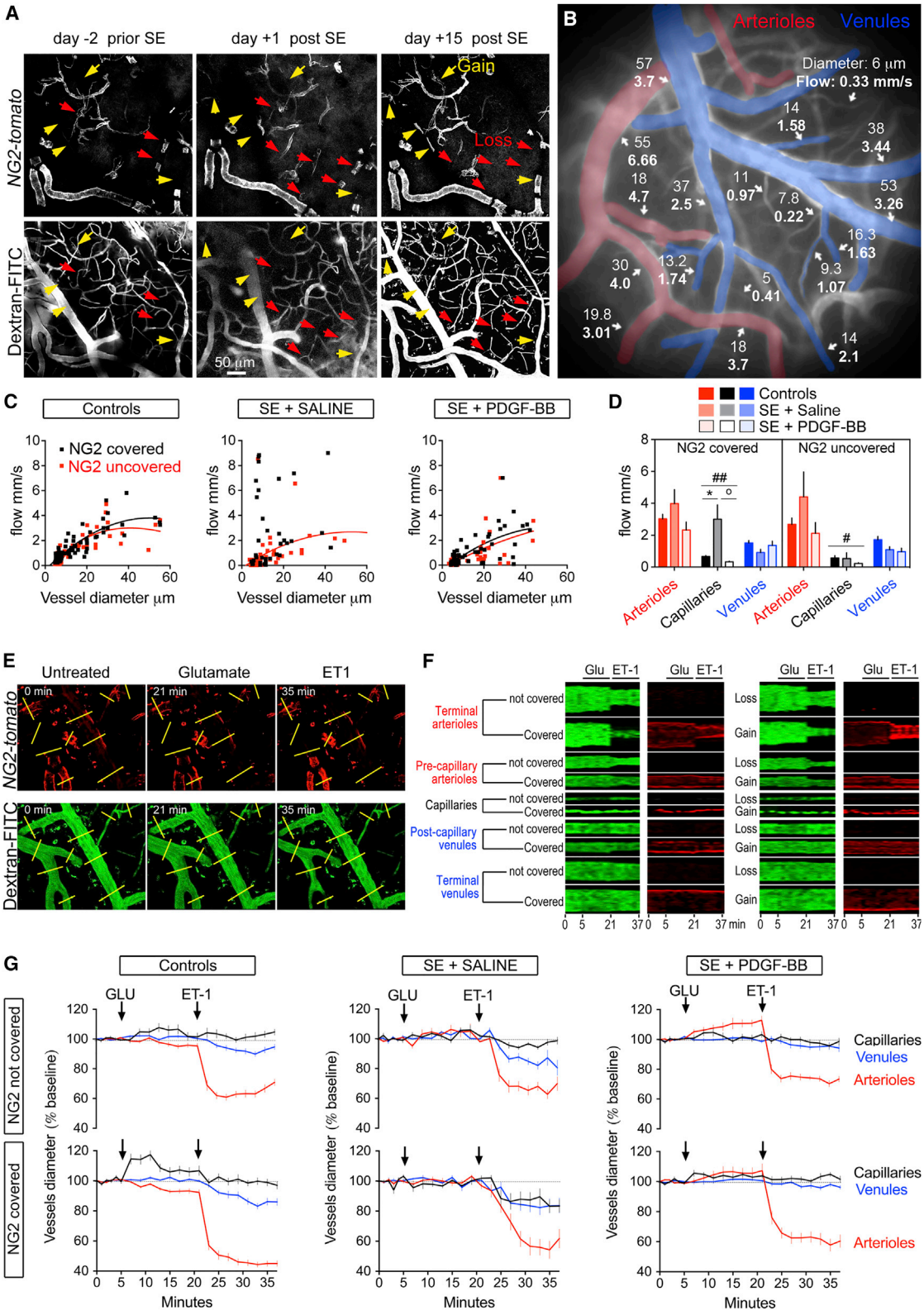

Figure 5. Impact of Mural Cell Remodeling on Vessel Tonus and Blood Flow

(A) Example of a cortical field imaged repeatedly though a thinned skull window to identify vessels with *NG2-tomato* mural cell remodeling post-status epilepticus (see arrows).

(legend continued on next page)

downregulation of endomucin facilitates leukocyte adhesion in the inflamed tissues (Zahr et al., 2016).

Disease Modifying Effect of PDGF-BB Treatment

Constitutive activation of PDGFRβ in transgenic mice facilitated mural cell growth, increasing pericyte coverage mostly on veins and capillaries in brain and peripheral organs (Olson and Soriano, 2011). PDGF-BB is a protein that does not cross the healthy BBB (Kastin et al., 2003). The latter does not represent an issue, because post-status epilepticus, (1) vessel permeability is compromised, (2) leakage sites expose abluminal PDGFRβ targets, and (3) impermeability of BBB to PDGF-BB upon vessel repair limits unwanted side effects. We report that a single intravenous injection of PDGF-BB at the time of status epilepticus increased significantly p-PDGFRβ on cortical veins and arterioles equally. Growth of mural cells was more prominent on veins where the microbleeds were less abundant. This is consistent with PDGF-BB treatment that increased the number of endomucin$^+$ vessels in bone (Xie et al., 2014). Blockade of PDGF-BB signaling in the context of inflammation increased leakiness of post-capillary venules (Fuxe et al., 2011), where downregulation of endomucin facilitates leukocyte adhesion previously linked to epileptogenesis (Fabene et al., 2008).

Mechanistically, exogenous PDGF-BB should activate PDGFRβ signaling prominently in stellate pericytes where PDGFRβ is abundant, at least more than in VSMCs (Li et al., 2011). PDGF-BB ameliorated vessel health and reduced spontaneous EEG epileptiform activity during treatment in a mouse model that did not generate permanent seizures (Ben-Ari, 2012). This extends a previous study reporting anticonvulsive effects of PDGF-BB at 24 hr and up to 1 week after one injection in a genetic mouse model with permanent seizures (Masuda et al., 1996). Yet benefits of PDGF-BB administration are mitigated by the oncogenic nature of tyrosine kinase receptor overactivation, and possible off-target effects via PDGFRα that can lead to fibrosis (Olson and Soriano, 2009; Andrae et al., 2008).

In conclusion, we introduce mural cells as cellular players in experimental seizures and PDGFRβ as a potential pharmacological entry point to limit cerebrovascular dysfunction in epilepsy.

EXPERIMENTAL PROCEDURES

Animals

Animal experiments were carried out in accordance with the directive by the Council of the European Communities (86/609/EEC) and approved protocols (00846.01 and 00651.01) following institutional guidelines for the care and use of laboratory animals. Tg(Cspg4-cre)1Akik/J (stock 008533), Ai27(RCL-hChR2(H134R)/tdT)-D (stock 012567), and wild-type mice in a C57BL/6 background (Jackson Laboratory, Bar Harbor, MA, USA) were housed under a 12 hr light/dark cycle with unrestricted access to food and water. All efforts were made to minimize animal suffering and to reduce the number of mice used in each experiment.

Electrode Implantation and Seizure Induction

Male and female mice were implanted with surface electrodes atop the frontoparietal cortex at 2 months of age to monitor EEG activity (Pinnacle, Sarasota, FL, USA). Mice were allowed 2 weeks of recovery from surgery before induction of status epilepticus using an intraperitoneal injection of 25 mg/kg kainic acid (KA) (Sigma-Aldrich, Saint-Quentin, France) in PBS. Racine's scale (Racine, 1972) and EEG were used to monitor the number of status epilepticus, the duration of epileptiform events, and the number of spikes at induction (Ben-Ari, 2012). All mice presented in the study experienced generalized seizures with at least one status epilepticus at induction, with the exception of controls and mice with stage III or IV non-generalized seizures.

Encephalography

EEG activity was monitored for >100 hr distributed in 4 epochs (pre- and post-status epilepticus, 1–2 weeks, and 5–6 weeks). Mice were monitored (behavior + EEG) for at least 3 hr after injection of KA or saline and subsequently sorted into 2 groups: (1) generalized seizures characterized by at least 1 status epilepticus and convulsions and (2) non-generalized seizures without status epilepticus. EEG signals were acquired at 200 Hz, stored, and analyzed using Sirenia (Pinnacle, Sarasota, FL, USA). Dual video-EEG inspection permitted the exclusion of artifacts associated with sniffing, scratching, eating, drinking, chewing, self-grooming, and sleep. To identify spontaneous epileptiform activities, we used criteria previously described (Fisher et al., 2014): (1) a spontaneous epileptiform event has a typical EEG pattern associated with sudden behavioral arrest, (2) a spontaneous spike wave has a typical EEG pattern associated with involuntary jerking movements, and (3) a spontaneous seizure has a typical EEG pattern associated with or without convulsive behavioral responses.

Intravenous Injections

Mice were lightly sedated with isoflurane, and a drop of ophthalmic anesthetic was applied topically before retro-orbital sinus injection of the fluorescent dyes (100 mg/kg of 70-kDa dextran-FITC and 70-kDa dextran-Texas red, Sigma-Aldrich, Saint-Quentin, France; 150 mg/kg of 10-kDa dextran-Alexa

(B) Example of transcranial epifluorescence dual imaging of the pial cerebrovasculature (with 70-kDa dextran-Texas red) and mural cells (with *NG2-tomato*) 2 weeks post-status epilepticus. Images were taken at 800 Hz for arterioles and between 100 and 400 Hz for capillaries and venules to calculate the average blood flow (in millimeters per second) at locations on vessels where mural cells are remodeled post-status epilepticus. See Video S1.

(C) Blood flow velocity during a period of 10 s in vessels covered and not covered with NG2-*tomato*. n = 110 vessels in 3 control mice, n = 92 vessels in 3 status epilepticus + saline mice, and n = 127 vessels in 4 status epilepticus + PDGF-BB mice.

(D) Average velocity sorted by vessel subtype categories. Two-way ANOVA for the effect of status epilepticus and PDGF-BB $F_{(2,311)} = 12.18$, $p < 0.0001$; effect of vessel category $F_{(5,311)} = 23.74$, $p < 0.0001$; and interaction $F_{(10,311)} = 3.58$, $p = 0.0002$. Post hoc t test comparing controls and status epilepticus + saline groups, *$p = 0.011$; comparing saline and PDGF-BB groups, °$p < 0.0001$; and comparing controls and status epilepticus + PDGF-BB groups, ##$p < 0.0001$ and #$p = 0.016$. See Table S4.

(E) Time-lapse two-photon microscopy of a cortical subfield of (A) with mural cell remodeling, imaged through a craniotomy, permitting topical drug application. Images were taken for 5 min during baseline, for 15 min during stimulation with glutamate (100 μM), and for 15 min during stimulation with ET-1 (10 nM). Yellow lines indicate where vessel diameter was analyzed corresponding to sites of mural cell remodeling. See Videos S2 and S3.

(F) Changes of vessel diameter plotted as a function of time. Representative effects of glutamate and ET-1 at vessels covered (pre-existing or gain) or not covered (pre-existing or loss) with *NG2-tomato* mural cells.

(G) Group data (means ± SEM expressed as a percentage of baseline) sorted by vessel categories and by mural cell coverage. Two-way ANOVA for the effect of ET-1 at vessel subtypes $F_{(5,618)} = 168.9$, $p < 0.0001$, and its interaction with status epilepticus and PDGF-BB $F_{(25,618)} = 40.64$, $p < 0.0001$. n = 73 vessels in 3 control mice, n = 32 vessels in 3 status epilepticus + saline mice, and n = 39 vessels in 4 status epilepticus + PDGF-BB mice for vessels not covered with *NG2-tomato*. n = 68 vessels in 3 control mice, n = 20 vessels in 3 status epilepticus + saline mice, and n = 37 vessels in 4 status epilepticus + PDGF-BB mice for vessels covered with *NG2-tomato*.

Post hoc t test for the effect of ET-1, *$p < 0.001$, and for the effect of glutamate, #$p < 0.05$. See Figures S4C and S4D for statistical comparisons.

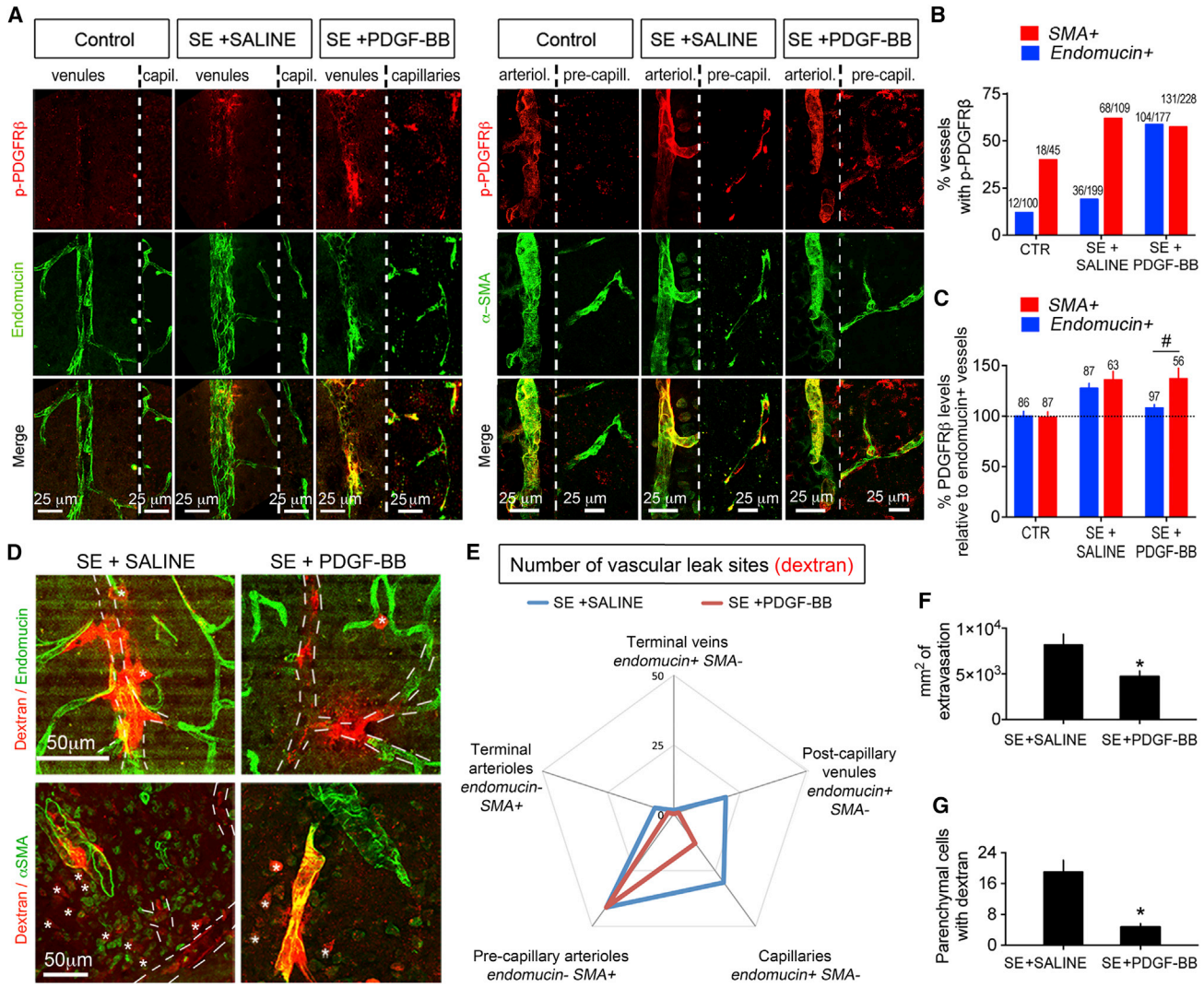

Figure 6. Venular Tropism of PDGF-BB Activity on PDGFRβ and Vessel Permeability Post-Status Epilepticus

(A) P-PDGFRβ (Y740-P) on vessel segments of cortical layers I–III labeled with endomucin (veins and capillaries) or α-SMA (arterioles).

(B) Proportion of endomucin-covered vessels or α-SMA-harboring vessels with p-PDGFRβ (Y740-P) in n = 4 controls, 5 status epilepticus + saline mice, and 6 status epilepticus + PDGF-BB mice.

(C) Proportion of endomucin-covered vessels or α-SMA-harboring vessels with PDGFRβ. Means ± SEM of n = 4 controls, 5 status epilepticus + saline mice, and 6 status epilepticus + PDGF-BB mice (unpaired t test comparing endomucin-covered vessels with α-SMA-harboring vessels in the status epilepticus + PDGF-BB group, #p = 0.0012). See Figures S5A–S5C.

(D) Extravasation of 10-kDa dextran injected into blood circulation at endomucin$^+$ and SMA$^+$ vessel segments in parietal cortex post-status epilepticus. Stars indicate parenchymal cells loaded with dextran.

(E) Percentage of extravasations sites sorted as a function of vessel markers and caliber: terminal vessels (25–50 μm), pre- or post-capillary vessels (8–25 μm), and capillaries (4–8 μm). n = 226 extravasation sites in the status epilepticus + saline group of 5 mice compared to n = 132 extravasation sites in the status epilepticus + PDGF-BB group of 6 mice.

(F) PDGF-BB reduces the surface of 10-kDa dextran extravasation sites in mouse cortex post-status epilepticus. Means ± SEM of n = 50 leaks/group (unpaired t test, *p = 0.01).

(G) PDGF-BB reduces the number of parenchymal cells loaded with 10-kDa dextran injected into blood circulation. Means ± SEM of n = 50 leaks/group (unpaired t test, *p < 0.0001). See Figures S5D and S5E.

See Table S5.

568, Applied Biosystems, Carlsbad, CA, USA; and 0.5% EB, Sigma-Aldrich, Saint-Quentin, France) or PDGF-BB (100 μg in saline, Sigma-Aldrich, Saint-Quentin, France). Volume of injection was always 50 μL. After 2 hr, the remaining circulating tracers were rinsed out of the circulation with PBS by transcardiac perfusion.

Transcranial Two-Photon Microscopy

Thin-skull preparation for transcranial *in vivo* imaging was performed as previously described (Arango-Lievano et al., 2016). All images were acquired with a Zeiss LSM710 two-photon microscope coupled to a Ti:sapphire laser (Spectra-Physics, Santa Clara, CA, USA) and a water

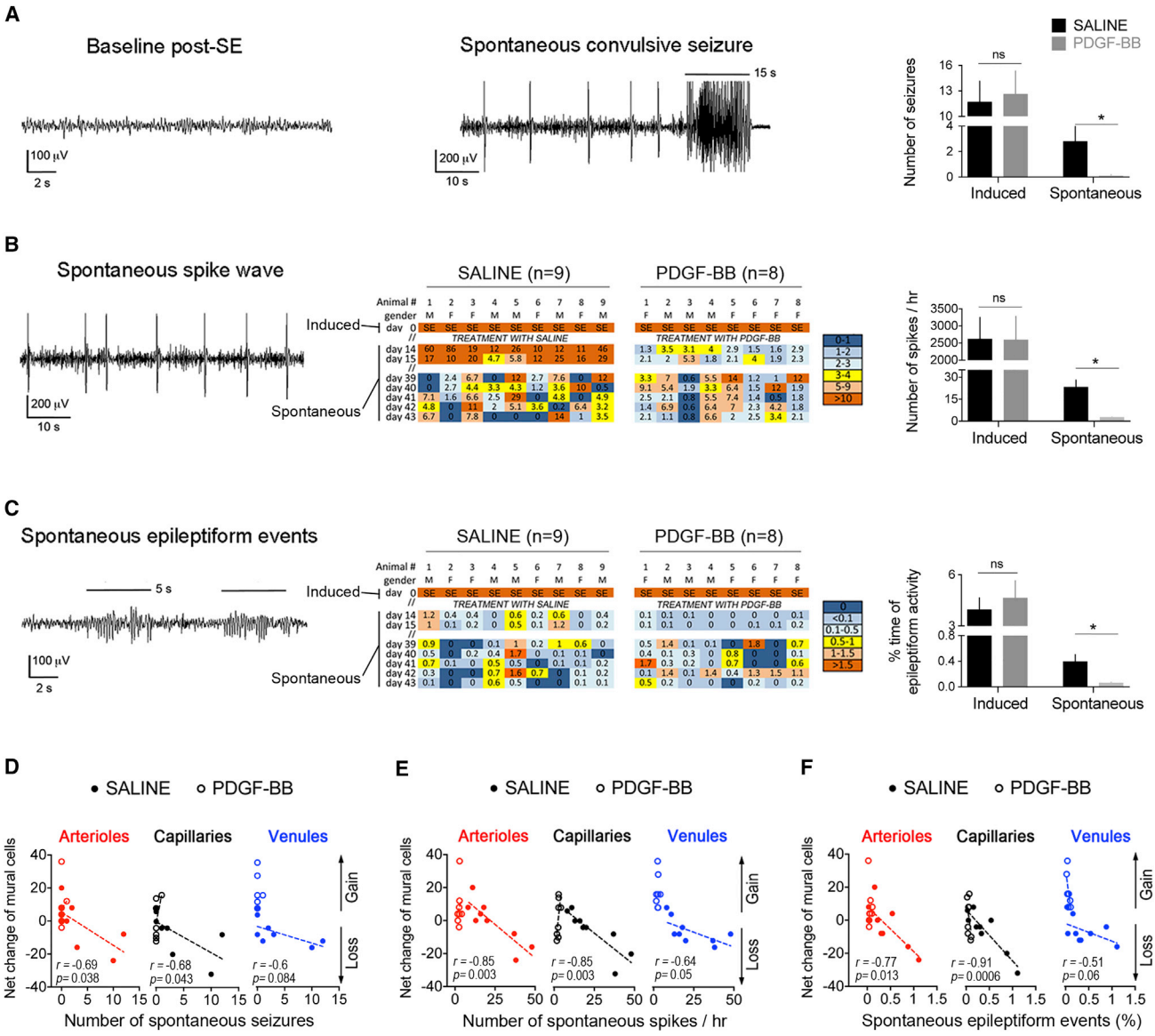

Figure 7. Reduction of Spontaneous EEG Activity with PDGF-BB Treatment

(A) Number of EEG seizures associated with convulsive behavior at induction (on day 0) and spontaneous after treatment with PDGF-BB or saline (in week 2). Means ± SEM of n = 10 mice/group (unpaired t test, *p = 0.036).

(B) Spikes presented as number per hour at induction and spontaneous in week 2. Means ± SEM of n = 9 status epilepticus + saline mice and 8 status epilepticus + PDGF-BB mice (unpaired t test, *p = 0.0012).

(C) Epileptiform events associated with behavioral arrest presented as a percentage of time recorded at induction and spontaneous in week 2. Means ± SEM of n = 9 status epilepticus + saline mice and 8 status epilepticus + PDGF-BB mice (unpaired t test, *p = 0.0218). See Table S6.

(D–F) Pearson correlation between the remodeling of NG2 mural cells (net gains and losses/square millimeter of cortex) and the number of spontaneous seizures (D), the number of spontaneous spikes (E), and the duration of epileptiform events (F). n = 9 status epilepticus + saline mice and 8 status epilepticus + PDGF-BB mice.

See Table S6.

immersion 20× objective (numerical aperture [NA] 1.0, Apochromat, Carl Zeiss, Iena, Germany) for optimal fluorophore excitation and emission separation. Excitation wavelengths avoided two-photon excitation wavelengths (880–920 nm) for channelrhodopsin-2 (ChR2) stimulation (Andrasfalvy et al., 2010) but were optimal for Tomato and dextran-FITC excitation (1040 and 780 nm, respectively). ChR2-dTomato could not be activated at these excitation wavelengths (Andrasfalvy et al., 2010). Laser power kept below 10 mW is not compatible with ChR2 stimulation but is necessary for non-damaging longitudinal studies. Images were taken at each image session for each mouse using a 1 µm step with a scanning dwell time of 2.55 µs/pixel. 1 µL of NeuroTrace 500/525 (Thermo Fisher Scientific, Waltham, MA, USA) was injected into parietal cortex layer 3, close to the region of interest, with a Hamilton syringe 24 hr before imaging as described (Damisah et al., 2017).

Reimaging of the Same Field of View in the Same Mice over Time

A detailed map of the pial vasculature was taken for subsequent relocation. Bone regrowth between imaging sessions is thinned using disposable ophthalmic surgical blades (Surgistar, USA). Skull is further thinned between imaging sessions down to 18–20 μm, allowing no more than 4 consecutive sessions to avoid cracking the skull (Arango-Lievano et al., 2016). Scalp is sutured and topped with topical antibiotic cream.

Transcranial Epifluorescence Microscopy of Blood Flow

Pial cerebrovascular blood flow is imaged through a thinned skull preparation with an epifluorescence Discovery V12 microscope (Carl Zeiss, Iena, Germany) equipped with 20× and 63× water objectives (Carl Zeiss, Iena Germany) and a digital camera (C11440 Orca-Flash 4.0, Hamamatsu, Barcelona, Spain) capturing images at 100 to 800 Hz. Dextran-Texas red (Sigma-Aldrich, Saint-Quentin, France), injected retro-orbitally, filled microcirculation but did not penetrate blood cells, permitting identification of their circulation. Imaging zones were defined by two-photon microscopy in which vessel coverage with *NG2-tomato* mural cells changed between sessions.

Time-Lapse Cerebrovascular Angiography

Two-photon microscopy was performed in terminal imaging sessions at open skull preparations to facilitate access of drugs to the pial surface of parietal cortex after surgical removal of meninges. Baseline vessel dynamics were captured in HEPES buffer (120 mM NaCl, 3.5 mM KCl, 0.4 mM KH2PO4, 15 mM glucose, 1.2 mM CaCl2, 5 mM NaHCO3, 1.2 mM Na2SO4, 20 mM HEPES [pH 7.4]) for 5 min before addition of 100 μM glutamate (Sigma, USA) for 15 min and subsequently 10 nM endothelin-1 (ET-1, Sigma, USA) for 15 min.

Image Analysis

Imaris 8.0 (Bitplane, Zurich, Switzerland) was used for 3D reconstruction of the field of view (volume = 500 × 500 × 250 μm) from a series of z stack images. Digital zoom values of 0.7 and 2.5 are necessary for reconstruction and future relocation. Mural cell skeletons were traced using the filaments tracer module of Imaris, which calculated the surface of vessels covered by NG2 mural cells. Sets of coordinates of the 3 imaging sessions are extracted with the Edlund method to align the coordinates with a stable reference point and further point-by-point analysis using MATLAB (MathWorks, Natick, MA, USA). Gains and losses of mural cells on vessel walls are measured by subtraction of signal between consecutive images. Specification among veins, capillaries, and arteries was performed based on NG2 mural cell morphology molecular markers endomucin (dela Paz and D'Amore, 2009) and α-SMA (Hill et al., 2015). Numbers of aneurysms, vasospasms, leakage spots, mural cell additions, or eliminations counted in fields of view were expressed as density per surface or volume as indicated. All images obtained from time-lapse imaging sessions were realigned with the ImageJ plugin RegStack to minimize artifacts of heartbeat pulsations. Images were stitched together using ImageJ. Vessel diameters were calculated at cross sections using the ImageJ plugin plot profile. Visualization of vessel diameter elasticity over time was obtained using the dynamic reslice plugin. Blood flow was analyzed from 10,000 images per field using an in-house MATLAB routine as described (Kim et al., 2012).

Immunohistochemistry

Mice were anesthetized with pentobarbital (50 mg/kg intraperitoneal [i.p.] injection, Ceva santé Animale, Libourne, France) and perfused at a rate of 3 mL/min through the ascending aorta with 30 mL of ice-cold 0.9% NaCl before decapitation. Brain hemisections were fixed with 4% ice-cold paraformaldehyde for 2 hr and equilibrated in 30% sucrose. Free-floating coronal sections rinsed in PBS were blocked in 5% normal goat or donkey serum, PBS, and 0.1% Triton X-100 for 2 hr at 25°C. Primary antibodies (1:500 Collagen IV, ab6586, Abcam, Cambridge, UK; 1:100 PDGFRβ, ab32570, Abcam, Cambridge, UK; 1:200 PDGFRβ [Y740-P], ab81301, Abcam, Cambridge, UK; 1:1,000 IBA1, ab5076, Abcam, Cambridge, UK; 1:1,000 GFAP, Z0334, Dako, Santa Clara, CA, USA; 1:500 endomucin, V5C7, Santa Cruz Biotechnology, Dallas, TX, USA; 1:500 α-SMA, clone 1A4, Sigma-Aldrich, Saint-Quentin, France; 1:100 cleaved caspase-3, Cell Signaling Technologies, USA; 1:500 KI67, ab15580, Abcam, Cambridge, UK) were incubated overnight. Alexa Fluor-conjugated secondary antibodies (1:2,000, Thermo Fisher Scientific, Waltham, MA, USA) were incubated for 2 hr at 25°C. Images were acquired with a LSM780 confocal microscope (Carl Zeiss, Iena, Germany) and a 20× water immersion objective. Excitation and acquisition parameters were unchanged during the acquisition of all images. Images were all taken in the parietal cortex underneath the two-photon imaging zone.

Brain Tissue Lysate Processing

Mice were anesthetized with pentobarbital (50 mg/kg intraperitoneal injection, Ceva santé Animale, Libourne, France) and perfused at a rate of 3 mL/min through the ascending aorta with 30 mL of 0.9% NaCl before decapitation. Parietal cortex from brain hemisections was obtained from 200-μm-thick sections dissected with a tissue punch (Stoelting, Wood Dale, IL, USA) and frozen in liquid nitrogen. Tissue was lysed in 10 mM Tris-HCl (pH 8.0), 150 mM NaCl, 1 mM EDTA, 10% glycerol, 1% nonidet P40 (NP40), 0.1% SDS, 0.1% Triton X-100 complemented with protease inhibitors, 1 mM Na_3VO_4, 10 mM NaF, and 10 nM calyculin A and was cleared from debris by centrifugation (14,000 rpm for 15 min) as described (Arango-Lievano et al., 2015).

Western Blot

Protein concentrations were measured with Bradford assay against BSA standards. Polyclonal antibodies against PDGFRβ (1:100, ab32570, Abcam, Cambridge, UK) were used for immunoprecipitation with protein A-conjugated magnetic beads (Life Technologies, Waltham, MA, USA) and western blot for detecting PDGFRβ [Y740-P] (1:200, ab81301, Abcam, Cambridge, UK) and pan-tyrosine-phosphorylation (pan-Y-P) (Santa Cruz Biotechnology, Dallas, TX, USA) by enhanced chemiluminescence (ECL) (Amersham). Densitometric analysis of grayscale images was performed with ImageJ.

Statistics

Parameters used to quantify imaging data include (1) vessel length covered by NG2 cells, (2) number of NG2 cells, (3) optical density in region of interest (ROI), (4) number of vessel anomalies, (5) vessel diameter, and (6) number or surface of vessel leaks that all were further sorted as a function of vessel caliber, mural cell subtype, and gains and losses over time. Parameters used to quantify EEG data include (1) number of seizures, (2) number of spikes, and (3) duration of epileptiform events that were all further sorted as induced or spontaneous. Representation of N for each figure is indicated in supplemental tables. All data collected in animals were from littermate controls and averaged per experimental groups. We used Student's t test to compare 2 groups or time points, Pearson correlation for linear associations between datasets with Prism 6.0 (GraphPad, La Jolla, CA, USA). The R^2 value determined the best linear fit of data. We used a factorial ANOVA to compare multiple groups, using status epilepticus, PDGF-BB, and vessel subtypes as independent factors, followed by post hoc pairwise comparison with multiple t tests (Holm-Sidak method for corrections). All data are shown as means ± SEM unless indicated otherwise. Significance level is set at $\alpha \leq 0.05$. No data were removed from analyses including statistical outliers. Estimates of sample size were calculated by power analysis based on preliminary data. Sample size was chosen to ensure 80% power to detect the pre-specified effect size. But N may vary among time points, because longitudinal *in vivo* imaging of the same cortical volume is challenging, presenting unexpected issues: (1) angle of imaging volume, (2) imperfection of surgical thinned skull windows, (3) mice that scratched off the EEG electrodes, and (4) inappropriate injection of the retro-orbital fluorescent dye. Pre-established criteria for stopping data collection included (1) mice that scratched off the EEG electrodes, (2) mice reaching ethical endpoint limits, (3) unexpected mortality (e.g., several mice died due to anesthesia, because of seizure intensity, or immediately after KA injections), (4) crack of the thin-skull preparation that would cause unwanted inflammation, and (5) brains badly perfused and unusable for histology.

SUPPLEMENTAL INFORMATION

Supplemental Information includes five figures, six tables, and three videos and can be found with this article online at https://doi.org/10.1016/j.celrep.2018.03.110.

ACKNOWLEDGMENTS

The Inserm Avenir grant (to F.J.), Ligue Française contre l'epilepsie (to M.A.-L.), Fondation pour la Recherche sur le Cerveau (FRC) (to N.M. and F.J.), CURE Innovator Award (to N.M.), Agence Nationale de la Recherche (ANR-15-CE14-0012-01 to P.M.), and FRC "Espoir en tête 2015" (to P.M., N.M., and F.J.) financed this work. We thank IPAM (to P.F., C.L., and P.M.) and FranceBioImaging (ANR-10-INSB-04 to P.M.).

AUTHOR CONTRIBUTIONS

M.A.-L. and F.J. designed the methods, carried out all *in vivo* imaging studies, and wrote the manuscript. P.M. designed the setup for blood flow acquisition. M.A.-L. and C.L. performed the blood flow studies. B.B. implanted EEG electrodes. L.D.T.D.T., C.G., and F.J. carried out histology and biochemical studies. M.A.-L., C.G., L.D.T.D.T., P.F., and F.J. analyzed images and EEG data and interpreted results. N.M. designed the experimental epilepsy model. All authors reviewed and approved the final manuscript.

DECLARATION OF INTERESTS

The authors declare no competing interests.

Received: June 13, 2017
Revised: January 4, 2018
Accepted: March 22, 2018
Published: April 24, 2018

REFERENCES

Andrae, J., Gallini, R., and Betsholtz, C. (2008). Role of platelet-derived growth factors in physiology and medicine. Genes Dev. *22*, 1276–1312.

Andrasfalvy, B.K., Zemelman, B.V., Tang, J., and Vaziri, A. (2010). Two-photon single-cell optogenetic control of neuronal activity by sculpted light. Proc. Natl. Acad. Sci. USA *107*, 11981–11986.

Arango-Lievano, M., Lambert, W.M., Bath, K.G., Garabedian, M.J., Chao, M.V., and Jeanneteau, F. (2015). Neurotrophic-priming of glucocorticoid receptor signaling is essential for neuronal plasticity to stress and antidepressant treatment. Proc. Natl. Acad. Sci. USA *112*, 15737–15742.

Arango-Lievano, M., Giannoni, P., Claeysen, S., Marchi, N., and Jeanneteau, F. (2016). Longitudinal In Vivo Imaging of the Cerebrovasculature: Relevance to CNS Diseases. J. Vis. Exp. *118*, e54796.

Armulik, A., Genové, G., Mäe, M., Nisancioglu, M.H., Wallgard, E., Niaudet, C., He, L., Norlin, J., Lindblom, P., Strittmatter, K., et al. (2010). Pericytes regulate the blood-brain barrier. Nature *468*, 557–561.

Armulik, A., Genové, G., and Betsholtz, C. (2011). Pericytes: developmental, physiological, and pathological perspectives, problems, and promises. Dev. Cell *21*, 193–215.

Attwell, D., Buchan, A.M., Charpak, S., Lauritzen, M., Macvicar, B.A., and Newman, E.A. (2010). Glial and neuronal control of brain blood flow. Nature *468*, 232–243.

Awad, I., and Jabbour, P. (2006). Cerebral cavernous malformations and epilepsy. Neurosurg. Focus *21*, e7.

Bell, R.D., Winkler, E.A., Sagare, A.P., Singh, I., LaRue, B., Deane, R., and Zlokovic, B.V. (2010). Pericytes control key neurovascular functions and neuronal phenotype in the adult brain and during brain aging. Neuron *68*, 409–427.

Ben-Ari, Y. (2012). Kainate and temporal lobe epilepsies: 3 decades of progress. In Jasper's Basic Mechanisms of the Epilepsies, Fourth Edition, J.L. Noebels, M. Avoli, M.A. Rogawski, R.W. Olsen, and A.V. Delgado-Escueta, eds. (National Center for Biotechnology Information), pp. 432–453.

Blinder, P., Shih, A.Y., Rafie, C., and Kleinfeld, D. (2010). Topological basis for the robust distribution of blood to rodent neocortex. Proc. Natl. Acad. Sci. USA *107*, 12670–12675.

Chang, J.C., Shook, L.L., Biag, J., Nguyen, E.N., Toga, A.W., Charles, A.C., and Brennan, K.C. (2010). Biphasic direct current shift, haemoglobin desaturation and neurovascular uncoupling in cortical spreading depression. Brain *133*, 996–1012.

Cocito, L., Favale, E., and Reni, L. (1982). Epileptic seizures in cerebral arterial occlusive disease. Stroke *13*, 189–195.

Damisah, E.C., Hill, R.A., Tong, L., Murray, K.N., and Grutzendler, J. (2017). A fluoro-Nissl dye identifies pericytes as distinct vascular mural cells during *in vivo* brain imaging. Nat. Neurosci. *20*, 1023–1032.

Daneman, R., and Prat, A. (2015). The blood-brain barrier. Cold Spring Harb. Perspect. Biol. *7*, a020412.

Daneman, R., Zhou, L., Kebede, A.A., and Barres, B.A. (2010). Pericytes are required for blood-brain barrier integrity during embryogenesis. Nature *468*, 562–566.

Dehouck, M.P., Vigne, P., Torpier, G., Breittmayer, J.P., Cecchelli, R., and Frelin, C. (1997). Endothelin-1 as a mediator of endothelial cell-pericyte interactions in bovine brain capillaries. J. Cereb. Blood Flow Metab. *17*, 464–469.

dela Paz, N.G., and D'Amore, P.A. (2009). Arterial versus venous endothelial cells. Cell Tissue Res. *335*, 5–16.

Drew, P.J., Shih, A.Y., Driscoll, J.D., Knutsen, P.M., Blinder, P., Davalos, D., Akassoglou, K., Tsai, P.S., and Kleinfeld, D. (2010). Chronic optical access through a polished and reinforced thinned skull. Nat. Methods *7*, 981–984.

Fabene, P.F., Navarro Mora, G., Martinello, M., Rossi, B., Merigo, F., Ottoboni, L., Bach, S., Angiari, S., Benati, D., Chakir, A., et al. (2008). A role for leukocyte-endothelial adhesion mechanisms in epilepsy. Nat. Med. *14*, 1377–1383.

Farrell, J.S., Colangeli, R., Wolff, M.D., Wall, A.K., Phillips, T.J., George, A., Federico, P., and Teskey, G.C. (2017). Postictal hypoperfusion/hypoxia provides the foundation for a unified theory of seizure-induced brain abnormalities and behavioral dysfunction. Epilepsia *58*, 1493–1501.

Fisher, R.S., Scharfman, H.E., and deCurtis, M. (2014). How can we identify ictal and interictal abnormal activity? Adv. Exp. Med. Biol. *813*, 3–23.

Friedman, A. (2011). Blood-brain barrier dysfunction, status epilepticus, seizures, and epilepsy: a puzzle of a chicken and egg? Epilepsia *52* (*Suppl 8*), 19–20.

Fuxe, J., Tabruyn, S., Colton, K., Zaid, H., Adams, A., Baluk, P., Lashnits, E., Morisada, T., Le, T., O'Brien, S., et al. (2011). Pericyte requirement for anti-leak action of angiopoietin-1 and vascular remodeling in sustained inflammation. Am. J. Pathol. *178*, 2897–2909.

Garbelli, R., de Bock, F., Medici, V., Rousset, M.C., Villani, F., Boussadia, B., Arango-Lievano, M., Jeanneteau, F., Daneman, R., Bartolomei, F., and Marchi, N. (2015). PDGFRβ(+) cells in human and experimental neuro-vascular dysplasia and seizures. Neuroscience *306*, 18–27.

Gorter, J.A., van Vliet, E.A., and Aronica, E. (2015). Status epilepticus, blood-brain barrier disruption, inflammation, and epileptogenesis. Epilepsy Behav. *49*, 13–16.

Hall, C.N., Reynell, C., Gesslein, B., Hamilton, N.B., Mishra, A., Sutherland, B.A., O'Farrell, F.M., Buchan, A.M., Lauritzen, M., and Attwell, D. (2014). Capillary pericytes regulate cerebral blood flow in health and disease. Nature *508*, 55–60.

Hartmann, D.A., Underly, R.G., Grant, R.I., Watson, A.N., Lindner, V., and Shih, A.Y. (2015). Pericyte structure and distribution in the cerebral cortex revealed by high-resolution imaging of transgenic mice. Neurophotonics *2*, 041402.

He, L., Vanlandewijck, M., Raschperger, E., Andaloussi Mäe, M., Jung, B., Lebouvier, T., Ando, K., Hofmann, J., Keller, A., and Betsholtz, C. (2016). Analysis of the brain mural cell transcriptome. Sci. Rep. *6*, 35108.

Hill, R.A., Tong, L., Yuan, P., Murikinati, S., Gupta, S., and Grutzendler, J. (2015). Regional Blood Flow in the Normal and Ischemic Brain Is Controlled by Arteriolar Smooth Muscle Cell Contractility and Not by Capillary Pericytes. Neuron *87*, 95–110.

Kastin, A.J., Akerstrom, V., Hackler, L., and Pan, W. (2003). Different mechanisms influencing permeation of PDGF-AA and PDGF-BB across the blood-brain barrier. J. Neurochem. *87*, 7–12.

Keller, A., Westenberger, A., Sobrido, M.J., García-Murias, M., Domingo, A., Sears, R.L., Lemos, R.R., Ordoñez-Ugalde, A., Nicolas, G., da Cunha, J.E., et al. (2013). Mutations in the gene encoding PDGF-B cause brain calcifications in humans and mice. Nat. Genet. *45*, 1077–1082.

Kim, T.N., Goodwill, P.W., Chen, Y., Conolly, S.M., Schaffer, C.B., Liepmann, D., and Wang, R.A. (2012). Line-scanning particle image velocimetry: an optical approach for quantifying a wide range of blood flow speeds in live animals. PLoS ONE *7*, e38590.

Kisler, K., Nelson, A.R., Rege, S.V., Ramanathan, A., Wang, Y., Ahuja, A., Lazic, D., Tsai, P.S., Zhao, Z., Zhou, Y., et al. (2017). Pericyte degeneration leads to neurovascular uncoupling and limits oxygen supply to brain. Nat. Neurosci. *20*, 406–416.

Lagraoui, M., Latoche, J.R., Cartwright, N.G., Sukumar, G., Dalgard, C.L., and Schaefer, B.C. (2012). Controlled cortical impact and craniotomy induce strikingly similar profiles of inflammatory gene expression, but with distinct kinetics. Front. Neurol. *3*, 155.

Li, L., Blumenthal, D.K., Terry, C.M., He, Y., Carlson, M.L., and Cheung, A.K. (2011). PDGF-induced proliferation in human arterial and venous smooth muscle cells: molecular basis for differential effects of PDGF isoforms. J. Cell. Biochem. *112*, 289–298.

Lindahl, P., Johansson, B.R., Levéen, P., and Betsholtz, C. (1997). Pericyte loss and microaneurysm formation in PDGF-B-deficient mice. Science *277*, 242–245.

Liwnicz, B.H., Leach, J.L., Yeh, H.S., and Privitera, M. (1990). Pericyte degeneration and thickening of basement membranes of cerebral microvessels in complex partial seizures: electron microscopic study of surgically removed tissue. Neurosurgery *26*, 409–420.

Masuda, Y., Miura, N., Kawarada, Y., Kawagoe, M., Shimizu, T., Sugiyama, T., and Hishikawa, Y. (1996). Platelet-derived growth factor B-chain homodimer suppressing a convulsion of epilepsy model mouse El. Biochem. Biophys. Res. Commun. *223*, 60–63.

Ogura, S., Kurata, K., Hattori, Y., Takase, H., Ishiguro-Oonuma, T., Hwang, Y., Ahn, S., Park, I., Ikeda, W., Kusuhara, S., et al. (2017). Sustained inflammation after pericyte depletion induces irreversible blood-retina barrier breakdown. JCI Insight *2*, e90905.

Olson, L.E., and Soriano, P. (2009). Increased PDGFRalpha activation disrupts connective tissue development and drives systemic fibrosis. Dev. Cell *16*, 303–313.

Olson, L.E., and Soriano, P. (2011). PDGFRβ signaling regulates mural cell plasticity and inhibits fat development. Dev. Cell *20*, 815–826.

Ouyang, L., Zhang, K., Chen, J., Wang, J., and Huang, H. (2018). Roles of platelet-derived growth factor in vascular calcification. J. Cell. Physiol. *233*, 2804–2814.

Park, D.Y., Lee, J., Kim, J., Kim, K., Hong, S., Han, S., Kubota, Y., Augustin, H.G., Ding, L., Kim, J.W., et al. (2017). Plastic roles of pericytes in the blood-retinal barrier. Nat. Commun. *8*, 15296.

Paukert, M., and Bergles, D.E. (2012). Reduction of motion artifacts during *in vivo* two-photon imaging of brain through heartbeat triggered scanning. J. Physiol. *590*, 2955–2963.

Peppiatt, C.M., Howarth, C., Mobbs, P., and Attwell, D. (2006). Bidirectional control of CNS capillary diameter by pericytes. Nature *443*, 700–704.

Pinto, A., Sahin, M., and Pearl, P.L. (2016). Epileptogenesis in neurocutaneous disorders with focus in Sturge Weber syndrome. F1000Res. *5*, 370.

Proebstl, D., Voisin, M.B., Woodfin, A., Whiteford, J., D'Acquisto, F., Jones, G.E., Rowe, D., and Nourshargh, S. (2012). Pericytes support neutrophil subendothelial cell crawling and breaching of venular walls *in vivo*. J. Exp. Med. *209*, 1219–1234.

Racine, R.J. (1972). Modification of seizure activity by electrical stimulation. II. Motor seizure. Electroencephalogr. Clin. Neurophysiol. *32*, 281–294.

Sweeney, M.D., Ayyadurai, S., and Zlokovic, B.V. (2016). Pericytes of the neurovascular unit: key functions and signaling pathways. Nat. Neurosci. *19*, 771–783.

van Vliet, E.A., da Costa Araújo, S., Redeker, S., van Schaik, R., Aronica, E., and Gorter, J.A. (2007). Blood-brain barrier leakage may lead to progression of temporal lobe epilepsy. Brain *130*, 521–534.

Whiteus, C., Freitas, C., and Grutzendler, J. (2014). Perturbed neural activity disrupts cerebral angiogenesis during a postnatal critical period. Nature *505*, 407–411.

Winkler, E.A., Bell, R.D., and Zlokovic, B.V. (2010). Pericyte-specific expression of PDGF beta receptor in mouse models with normal and deficient PDGF beta receptor signaling. Mol. Neurodegener. *5*, 32.

Winkler, E.A., Bell, R.D., and Zlokovic, B.V. (2011). Central nervous system pericytes in health and disease. Nat. Neurosci. *14*, 1398–1405.

Winkler, E.A., Sengillo, J.D., Bell, R.D., Wang, J., and Zlokovic, B.V. (2012). Blood-spinal cord barrier pericyte reductions contribute to increased capillary permeability. J. Cereb. Blood Flow Metab. *32*, 1841–1852.

Xie, H., Cui, Z., Wang, L., Xia, Z., Hu, Y., Xian, L., Li, C., Xie, L., Crane, J., Wan, M., et al. (2014). PDGF-BB secreted by preosteoclasts induces angiogenesis during coupling with osteogenesis. Nat. Med. *20*, 1270–1278.

Xu, H.T., Pan, F., Yang, G., and Gan, W.B. (2007). Choice of cranial window type for *in vivo* imaging affects dendritic spine turnover in the cortex. Nat. Neurosci. *10*, 549–551.

Zahr, A., Alcaide, P., Yang, J., Jones, A., Gregory, M., dela Paz, N.G., Patel-Hett, S., Nevers, T., Koirala, A., Luscinskas, F.W., et al. (2016). Endomucin prevents leukocyte-endothelial cell adhesion and has a critical role under resting and inflammatory conditions. Nat. Commun. *7*, 10363.